Am J Physiol Lung Cell Mol Physiol 316: L1141–L1149, 2019.
First published March 25, 2019; doi:10.1152/ajplung.00032.2019.

RAPID REPORT

Development of solitary chemosensory cells in the distal lung after severe influenza injury

Chetan K. Rane,[1] Sergio R. Jackson,[1] Christopher F. Pastore,[1] Gan Zhao,[1] Aaron I. Weiner,[1] Neil N. Patel,[2] De'Broski R. Herbert,[1]* Noam A. Cohen,[2,3,4]* and Andrew E. Vaughan[1,5]*

[1]*School of Veterinary Medicine, University of Pennsylvania, Philadelphia, Pennsylvania;* [2]*Department of Otorhinolaryngology-Head and Neck Surgery, University of Pennsylvania Perelman School of Medicine, Philadelphia, Pennsylvania;* [3]*Monell Chemical Senses Center, Philadelphia, Pennsylvania;* [4]*Philadelphia Veterans Affairs Medical Center Surgical Service, Philadelphia, Pennsylvania; and* [5]*Institute for Regenerative Medicine, University of Pennsylvania, Philadelphia, Pennsylvania*

Submitted 22 January 2019; accepted in final form 18 March 2019

Rane CK, Jackson SR, Pastore CF, Zhao G, Weiner AI, Patel NN, Herbert DR, Cohen NA, Vaughan AE. Development of solitary chemosensory cells in the distal lung after severe influenza injury. *Am J Physiol Lung Cell Mol Physiol* 316: L1141–L1149, 2019. First published March 25, 2019; doi:10.1152/ajplung.00032.2019.—H1N1 influenza virus infection induces dramatic and permanent alveolar remodeling mediated by $p63^+$ progenitor cell expansion in both mice and some patients with acute respiratory distress syndrome. This persistent lung epithelial dysplasia is accompanied by chronic inflammation, but the driver(s) of this pathology are unknown. This work identified de novo appearance of solitary chemosensory cells (SCCs), as defined by the tuft cell marker doublecortin-like kinase 1, in post-influenza lungs, arising in close proximity with the dysplastic epithelium, whereas uninjured lungs are devoid of SCCs. Interestingly, fate mapping demonstrated that these cells are derived from p63-expressing lineage-negative progenitors, the same cell of origin as the dysplastic epithelium. Direct activation of SCCs with denatonium + succinate increased plasma extravasation specifically in post-influenza virus-injured lungs. Thus we demonstrate the previously unrecognized development and activity of SCCs in the lung following influenza virus infection, implicating SCCs as a central feature of dysplastic remodeling.

chemosensory; inflammation; influenza; progenitor; tuft

INTRODUCTION

Infection with highly virulent strains of influenza A can cause viral pneumonia and respiratory distress (28), with as many as 500,000 deaths reported worldwide annually (33a). While most patients recover, there is increasing evidence that, despite viral clearance, chronic pathology and diminished lung function persist in many individuals (2, 9, 18). Both mice and humans exhibit dramatic lung regeneration upon injury induced by influenza virus, involving a heterogeneous assemblage of epithelial progenitor cells (10, 30, 32, 34, 36). Moderately injured alveolar parenchyma is reconstituted by alveolar type 2 (AT2) cells (36) and $Sox2^+$ distal airway cells (32, 34), resulting in restoration of functional AT2 and alveolar type 1 (AT1) cells. However, there is also massive expansion of a rare subpopulation of cells, $\Delta Np63^+$ lineage-negative progenitors, after severe influenza virus-induced injury. These cells, originally residing in the intrapulmonary airways, respond to hypoxia in severely damaged alveolar areas and initiate a bronchiolization/remodeling program characterized by cytokeratin 5 (Krt5) expression (32, 34, 35). This phenomenon is particularly dramatic given that Krt5 expression is normally restricted to basal cells in the trachea and mainstem bronchi. While expansion of these cells into the alveoli likely imparts a short-term benefit through restoration of barrier function (36), $Krt5^+$ cells rarely resolve into AT2 or AT1 cells. Instead, they form dysplastic "epithelial scars" that persist through the lifespan of mice and, likely, humans (30, 32) and seemingly do not contribute to pulmonary gas exchange functions.

We and others have shown that the lung epithelial dysplasia in mice after infection with influenza virus A/H1N1/PR/8 is associated with chronic inflammation (7, 22). The coincidence of $Krt5^+$ dysplastic epithelial cells and inflammatory cells suggests cross talk between the epithelial and immune compartments and the possibility that inflammation drives and/or maintains epithelial dysplasia. This inflammation was recently described as a type 2 (Th2) immune environment, characterized by increased IL-13 and IL-33 production (7, 20).

Based on our recent work demonstrating that solitary chemosensory cells (SCCs) in human upper airway produce IL-25 and expand in response to IL-13 (8, 25) and work by others demonstrating that related intestinal tuft cells respond to pathogen infection by producing type 2 cytokines (4, 33), we hypothesized that SCCs could be involved in some aspect of influenza virus-induced lung injury. Our data show that SCCs, also known as tuft or brush cells, were indeed ectopically present in the areas of remodeled alveoli induced by influenza viral damage. This finding is particularly striking, given that SCCs do not exist distal to the trachea in uninjured mice. SCCs have been previously identified as epithelial chemosensors in the sinonasal mucosa that respond to "bitter" irritants to promote local neurogenic inflammation in the mouse (26) and drive release of antimicrobial peptides in the human (13, 14). In the intestine, tuft cells represent a key node of the Th2

* D. R. Herbert, N. A. Cohen, and A. E. Vaughan contributed equally to this work as senior authors.

Address for reprint requests and other correspondence: A. E. Vaughan, University of Pennsylvania School of Veterinary Medicine, 3800 Spruce St., Old Vet 372E, Philadelphia, PA 19104 (e-mail: andrewva@vet.upenn.edu).

immune circuit responsible for IL-25 production and subsequent epithelial remodeling and host immunity (4, 5, 27, 33). Tuft cells have also been identified in the trachea (here called brush cells), where they orchestrate inflammation in response to leukotrienes (1). Here we elucidate the origin of ectopic lung SCCs, examine their tuft cell-like character, and demonstrate their ability to induce changes in both physiology and inflammation in the lung following SCC-restricted receptor-mediated activation. This work implicates SCCs as a central feature of viral infection-induced lung pathology.

MATERIALS AND METHODS

Animals and treatment. All animal procedures were approved by the Institutional Animal Care and Use Committee of the University of Pennsylvania. p63-CreERT2 (12), Ai14-tdTomato (19), and Trpm5-GFP (3) mice are described elsewhere. For all experiments, 6- to 8-wk-old C57BL/6 mice of both sexes were used in equal proportions. For all animal studies, no statistical method was used to predetermine sample size. The experiments were not randomized, and the investigators were not blinded to allocation during experiments and outcome assessment. For influenza virus infection, influenza virus A/H1N1/PR/8 was administered intranasally to <25-g mice at 75 median tissue culture infectious dose ($TCID_{50}$) units and to >25-g mice at 100 $TCID_{50}$ units. Briefly, mice were anesthetized with 3.5% isoflurane for 5 min until agonal breathing was observed. Virus dissolved in 30 μl of PBS was pipetted onto the nostrils of anesthetized mice, whereupon they aspirated the fluid directly into their lungs. After this protocol, infected mice lose, on average, 22% of body weight by 7 days, and their peripheral capillary oxygen saturation drops to 72.5 ± 9.0% by post-infection *day 11*.

Lineage tracing. Three doses (0.25 mg/g body wt) of tamoxifen dissolved in 50 μl of corn oil were administered via intraperitoneal injection to p63-CreERT2/tdTomato mice (a gift from Dr. Jianming Xu, Baylor College of Medicine) for determination of the cell of origin for post-influenza doublecortin-like kinase 1 (DCLK1)-positive ($DCLK1^+$) cells. After 3 wk for tamoxifen clearance, the mice were infected as described above. Fidelity of lineage tracing in these mice has been previously described (34, 35).

Tissue preparation and immunofluorescence. Freshly dissected mouse lungs were inflated with 4% paraformaldehyde (PFA) for 1 h at room temperature. Fixed lungs were washed by multiple changes of PBS over the course of 1 h at room temperature and incubated overnight in 30% sucrose with shaking at 4°C and for 2 h in 15% sucrose-50% optimal cutting temperature compound (Fisher HealthCare) at room temperature. Finally, fixed lungs were embedded in optimal cutting temperature compound by flash freezing with dry ice and ethanol. Cryosections (7 μm thick) were cut and fixed for an additional 5 min in 4% PFA at room temperature, incubated three times at 10-min intervals with 1% sodium borohydride (Sigma-Aldrich) in PBS to reduce aldehyde-induced background fluorescence, and subsequently blocked and stained in PBS + 1% BSA (Affymetrix), 5% nonimmune horse serum, 0.1% Triton X-100, and 0.02% sodium azide.

The following antibodies were used for immunofluorescence: rabbit anti-DCLK1 (1:800 dilution; catalog no. ab37994, Abcam) (1, 5), chicken anti-Krt5 (1:200 dilution; catalog no. 905901, BioLegend) (32, 34), rabbit anti-surfactant protein C (1:2,000 dilution; catalog no. ab3786, Millipore) (32, 34–36), rabbit anti-trefoil factor 2 (Tff2, 1:100 dilution; 13681-1-AP, Proteintech) (29), and mouse anti-mucin 5ac (Muc5ac, 1:100 dilution; catalog no. 45M1, Invitrogen) (29).

Quantification of immunofluorescence. To quantify $Krt5^+$ area, mosaic images covering the whole lobes were generated from multiple ×10 fields captured on an upright fluorescence microscope (model DMi8, Leica) and tiled in LAS X software (Leica). The $Krt5^+$ areas and total areas were measured by manual outlining of stained areas in ImageJ and calculation of area ratios. At least three sections, each containing two to three individual lobes and separated by >300-μm depth, were quantified for each mouse.

To quantify p63-CreERT2 trace of $DCLK1^+$ cells post-influenza, images were captured as described above, and the total number of $DCLK1^+$ cells was manually counted and assessed for lineage trace by determination of Cre-activated tdTomato (303 $DCLK1^+$ cells; 301 $DCLK1^+$/tdTomato) coexpression.

Hematoxylin-eosin staining. Lung tissue sections fixed with 4% PFA were stained with hematoxylin and eosin by the Penn Vet Comparative Pathology core.

Periodic acid-Schiff and Alcian blue staining. Alcian blue/periodic acid-Schiff staining was performed by the Penn Vet Comparative Pathology core as follows. Slides were stained with Alcian blue dye for 30 min and rinsed under running water for 2 min and then with distilled water for 30 s. Slides were then incubated for 10 min in 0.5% periodic acid at 4°C, rinsed under running water for 5 min, and incubated for 10 min in Schiff reagent. Finally, slides were placed in hot water for 2 min, washed again for 2 min in distilled water, counterstained with hematoxylin, dehydrated, and mounted. Bright-field images were acquired on an upright fluorescence microscope (model DMi8, Leica).

Bronchoalveolar lavage. The trachea was exposed, and a 20-gauge catheter was inserted for lavage. Cold PBS (1 ml) was instilled into the mouse lungs, and gentle aspiration was repeated three times. Cell count was immediately performed using a hemocytometer.

Cytospins and Diff-Quik counts. Bronchoalveolar lavage fluid (BALF) was centrifuged at 550 *g* for 5 min, and the supernatant was transferred to separate tubes. The cells were resuspended in 4% PFA and fixed onto slides using a Cytospin centrifuge at 750 rpm for 4 min.

Hema3 stain kit (Fisherbrand) protocol was used to determine Diff-Quik cell counts.

RNA sequencing of $Krt5^+$ cells. Krt5-CreERT2/tdTomato-traced cells from post-infection *day 17* were isolated by fluorescence-activated cell sorting, and RNA was extracted using a ReliaPrep RNA Tissue Miniprep kit (Promega). cDNA synthesis/amplification, library preparation, and sequencing were carried out as described elsewhere (34).

Lung permeability assay. The lung permeability assay was performed as described elsewhere (26) with the following modifications. An orotracheal spray nozzle was used to administer 50 μl of PBS or denatonium (10 mM) + succinate (10 mM) in PBS intratracheally to mice anesthetized with vaporized isoflurane (see above). After 5 min, 100 μl of FITC-dextran (3–5 kDa; Sigma) were injected intravenously. After 15 min to allow fluorescence-labeled dextran to circulate in the blood, BALF was collected, cell count was performed, and fluorescence intensity was determined using a spectrophotometer.

Chronic administration of denatonium + succinate. To investigate the significance of repeated stimulation of SCCs, 50 μl of PBS or denatonium (10 mM) + succinate (10 mM) in PBS were administered intratracheally once every day for 7 days. Then BALF was collected and lungs were fixed as described above. The total number of $DCLK1^+$ cells within a $Krt5^+$ area was manually counted and quantified.

Cell line identity. No cell lines were used in this study.

Statistical analyses. All statistical calculations were performed using GraphPad Prism. The Mann-Whitney test was used to determine significance. $P < 0.05$ was considered significant.

RESULTS

SCCs arise ectopically in post-influenza dysplastic lungs. Extensive alveolar damage and permanent epithelial dysplasia ensue after influenza A/H1N1/PR/8 infection (Fig. 1*A*) (32, 34, 36), but the underlying driver(s) remains obscure. Expansion of $Krt5^+$ dysplastic epithelial cells is accompanied by increased $CD45^+$ immune cells through ≥49 days

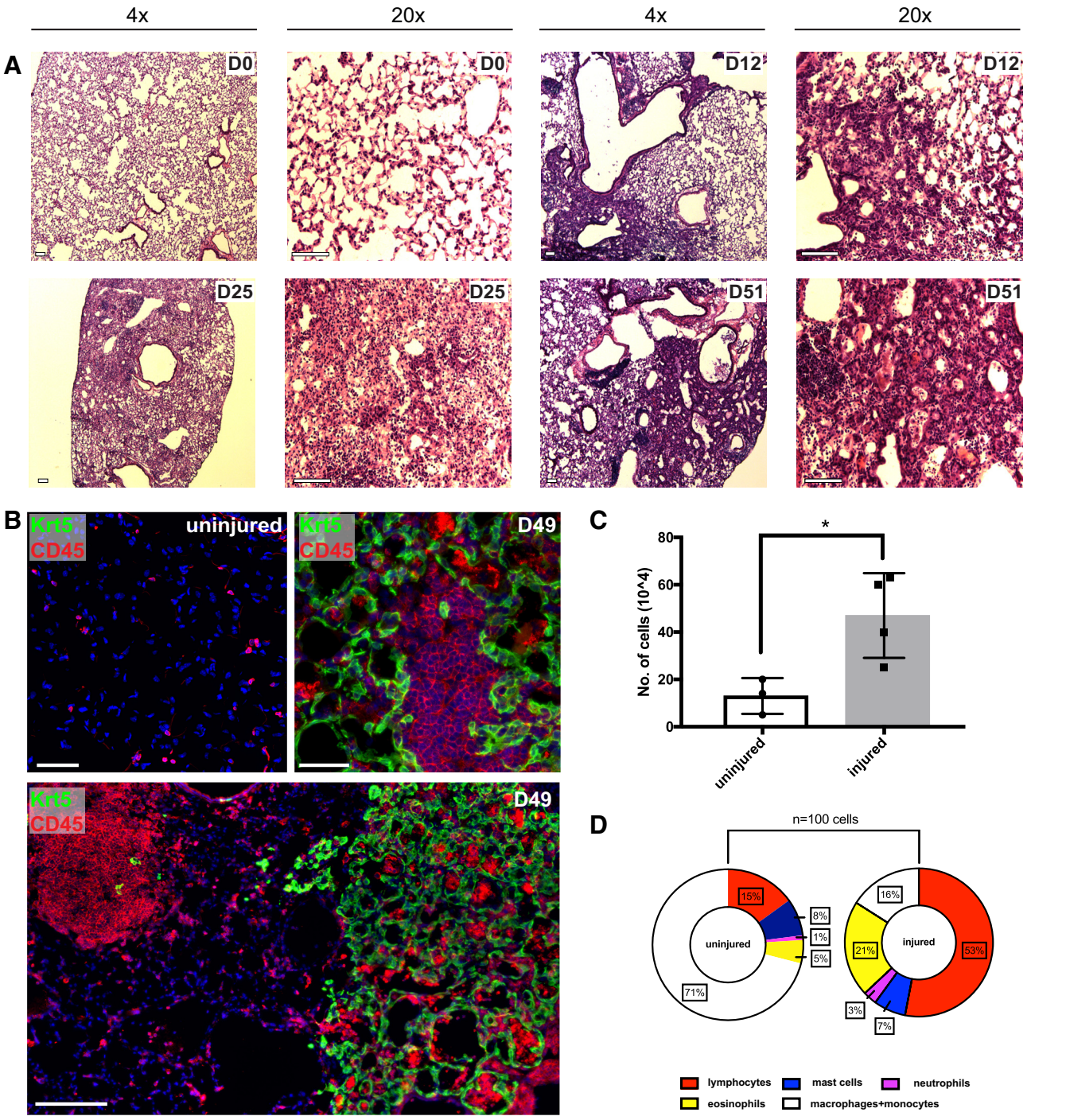

Fig. 1. Chronic inflammation and extensive alveolar damage in post-influenza lungs. *A*: hematoxylin-eosin staining of lung tissue sections on post-infection *days 0–51* indicates epithelial ablation and extensive alveolar damage. *B*: influenza virus infection results in cytokeratin 5 (Krt5)-positive ($Krt5^+$) cell expansion accompanied by increased $CD45^+$ immune cells up to post-infection *day 49*, while uninjured lungs demonstrate only normal resident immune cells and lack $Krt5^+$ cells. Scale bars, *A*, 100 μm; *B*, 50 μm. *C*: bronchoalveolar lavage fluid displays a significantly higher immune cell count in post-influenza (*days 25–51*) lungs. Values are means ± SE; $n = 3$ uninjured and 4 injured mice. *D*: bronchoalveolar lavage fluid cell composition post-influenza demonstrates increased lymphocyte and eosinophil counts, indicating inflammation. $^*P < 0.05$.

post-infection (Fig. 1*B*) compared with uninjured controls. Large aggregates of immune cells, similar in gross appearance to induced bronchus-associated lymphoid tissue, were commonly observed (22). Chronic inflammation was further supported by an increased number of immune cells in BALF collected from mice well past the primary immune response (Fig. 1*C*). Differential staining of BALF demonstrated increased percentages of lymphocytes and eosinophils in injured lungs (Fig. 1*D*). Furthermore, we observed increased periodic acid-Schiff and Alcian blue staining in dysplastic regions of the injured lungs, indicating mucous metaplasia (Fig. 2*A*). This observation was further validated by in-

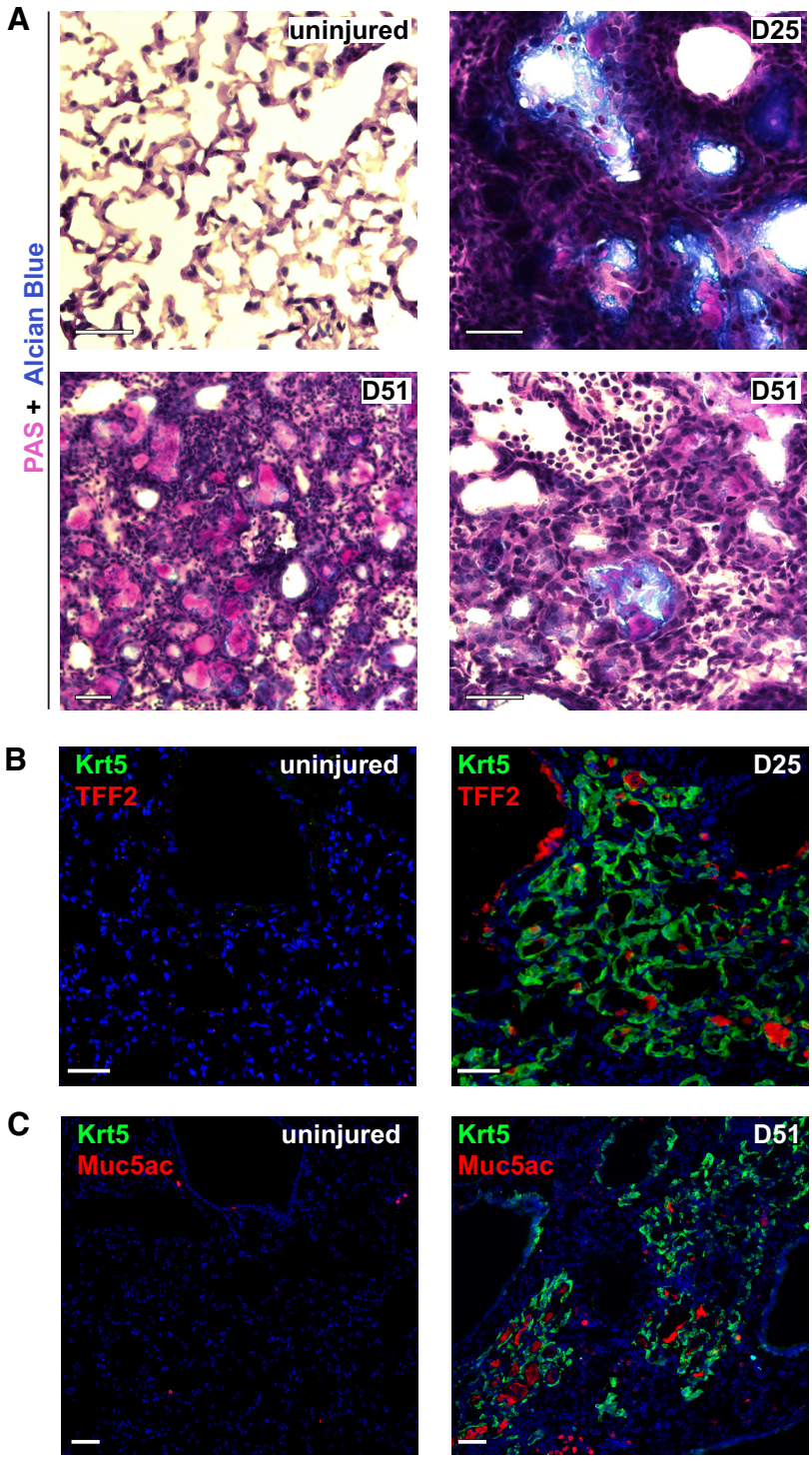

Fig. 2. Goblet cell hyperplasia in post-influenza lungs. *A*: periodic acid-Schiff (PAS)/Alcian blue staining indicates goblet cell hyperplasia in post-influenza (*days 25* and *51*) lungs. *B* and *C*: increased immunostaining for the goblet cell markers trefoil factor 2 (Tff2) and mucin 5ac (Muc5ac) in the lung at *days 25* and *51*, respectively. Krt5, cytokeratin 5. Scale bars, 50 μm.

creased immunostaining for the goblet cell markers Muc5ac and Tff2 (21) (Fig. 2, *B* and *C*).

To address whether SCCs might also arise in this environment, we utilized immunostaining for the conserved SCC/tuft cell/brush cell marker gene DCLK1. Strikingly, DCLK1$^+$ cells, with characteristic unipolar morphology, were found in close association with the dysplastic epithelium as early as post-infection *day 12*. SCCs increase in number through ~25 days post-infection and persisted even at late time points (*day 49*) (Fig. 3, *A* and *B*). Given that SCCs arise near Krt5$^+$ cells at all time points, we asked whether these cells might share a common cell of origin, as judged by fate-mapping analysis. We infected tamoxifen-treated p63-CreERT2/lsl-tdTomato mice in which p63$^+$ progenitor cells and their descendants are indelibly labeled by tdTomato expression. Nearly 100% of SCCs were labeled, indicating that they share a common origin with the dysplastic epithelium (Fig. 3, *C* and *D*).

To confirm the identity of influenza-associated SCCs, we examined RNA-sequencing expression data of Krt5-CreERT2 lineage-labeled cells isolated on post-infection *day 17* (34). This population, which contains Krt5$^+$ cells, as well as cells beginning to differentiate toward the various dysplasia-associated cell types, demonstrated increased expression of tuft cell/SCC-restricted genes [the tuft cell marker DCLK1 and tuft cell signaling genes transient receptor potential cation channel

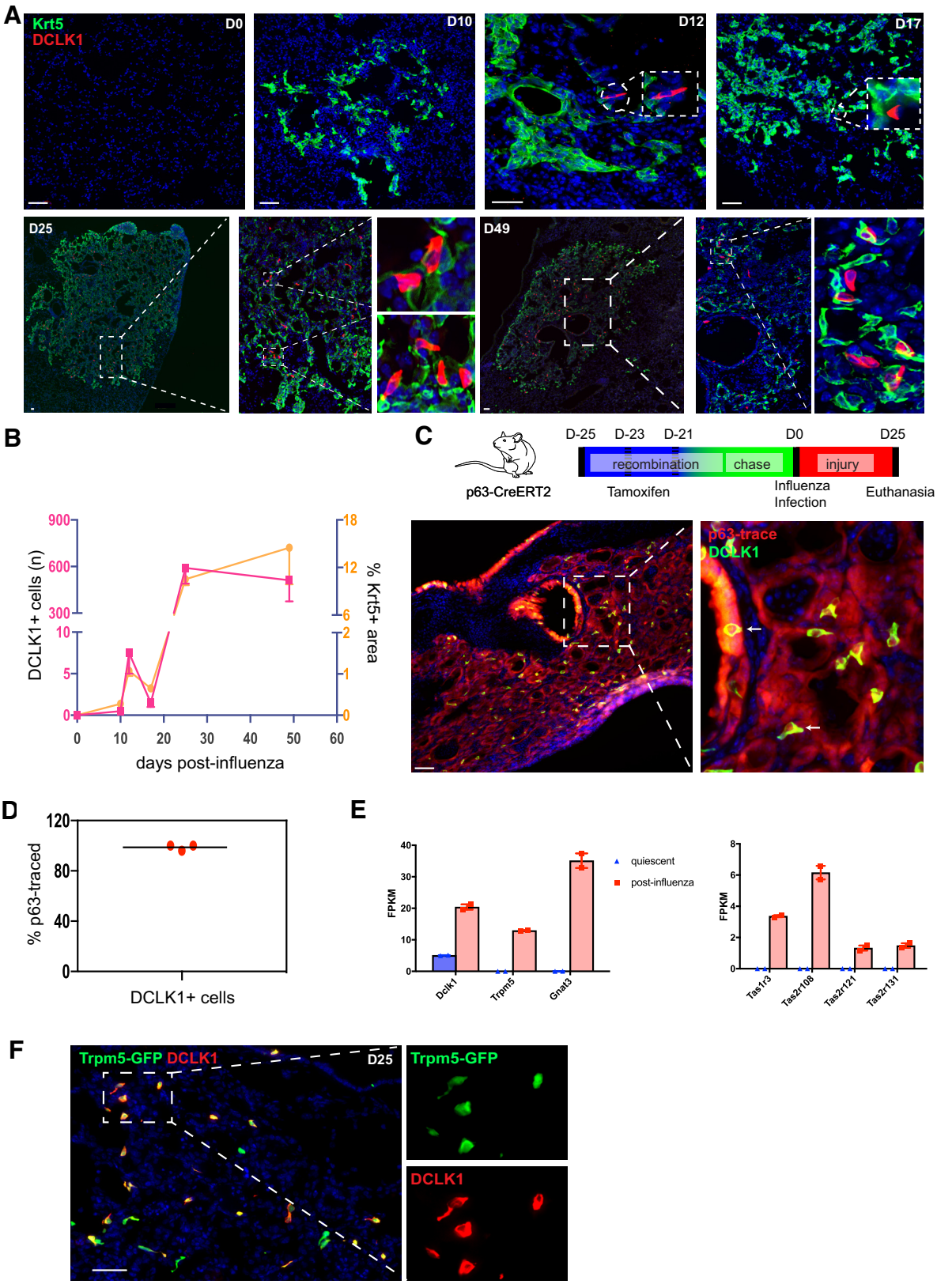

subfamily M member 5 (Trpm5) and G protein subunit-α transducin 3 (Gnat3)] (Fig. 3*E, left*), including multiple bitter taste receptors (Tas1r3, Tas2r108, Tas2r121, and Tas2r131) (Fig. 3*E, right*). In addition to corroborating the p63 lineage-trace data, these data confirm expression of many tuft cell/SCC-associated genes and imply a shared character with chemosensory cells in other tissues. To further validate the identity of SCCs in post-influenza lungs, we utilized Trpm5-GFP reporter mice in which green fluorescent protein (GFP) expression is restricted to SCCs and tuft cells (5, 16, 31). At post-infection *day 25*, we observed numerous GFP^+ cells in dysplastic regions. All $DCLK1^+$ cells observed were GFP^+, marking these cells as bona fide SCCs (Fig. 3*F*).

SCC activation promotes plasma extravasation in post-influenza lungs. To establish a functional role for SCCs within the distal lung post-influenza, we asked whether exposure to the SCC-activating ligands denatonium (13, 14, 26, 31) and succinate (15, 23, 27) could induce components of inflammation. We employed a lung permeability assay utilizing intravenous administration of FITC-dextran to determine whether SCC stimulation can induce plasma extravasation into the air space based on a prior model in the mouse upper airway (26). Indeed, combinatorial intratracheal administration of denatonium and succinate acutely increased lung permeability, as observed by a significant increase in FITC-dextran levels in BALF of injured, but not naïve, animals (Fig. 4*A*). These data indicate that SCC expansion enables the affected lung tissue to respond to activating ligands such as denatonium and succinate, resulting in plasma extravasation, as measured by increased permeability to FITC-dextran.

Intestinal tuft cells, upon activation, promote epithelial remodeling, resulting in more tuft cells (27). To examine whether a similar scenario occurs in the lungs, we administered denatonium + succinate to influenza-infected mice daily for 7 days. Long-term, repetitive activation of SCCs resulted in a significant increase in the number of $DCLK1^+$ cells (Fig. 4*B*), supporting a positive-feedback circuit that expands local SCC numbers post-infection.

DISCUSSION

In this study we demonstrate the appearance of ectopic SCCs in the distal lung after influenza virus-induced injury. These cells are entirely absent in uninjured lungs but develop adjacent to dysplastic ($Krt5^+$) epithelium. Fate mapping validated that SCCs arise from $p63^+$ lineage-negative progenitors, the same cell of origin as the $Krt5^+$ cells. This common parentage hints at a relationship between SCCs and lung epithelial dysplasia, whereby SCCs might promote the maintenance of dysplastic epithelium. The intestinal model in which tuft cell expansion simultaneously promotes Th2 inflammation and epithelial metaplasia (33) is entirely consistent with our contention.

Direct activation of SCCs by denatonium + succinate resulted in increased plasma extravasation into the air space, a hallmark of inflammation (26). It is possible that this effect on permeability is induced by SCC-mediated activation of a neurogenic inflammatory pathway, as occurs in the nasal cavity (16, 26). On the other hand, permeability changes could also result from SCC-derived Th2 cytokine stimulation, as observed in the intestinal tuft cell model. Future efforts should focus on precise definition of the molecular mechanisms by which SCC stimulation promotes inflammatory changes. It is also important to note that we analyzed a relatively broad time window for post-infection mice in Fig. 4*A*; we reasoned that since SCC numbers remained constant after post-infection *day 25*, mice past that point represent a reasonable cohort. In future studies, more precise time-course experiments should be performed to examine the effects of SCC stimulation as a function of time post-infection.

An important caveat of intratracheal administration of SCC ligands is that faulty technique could inadvertently activate brush cells in the upper trachea (present in naïve, uninjured mice), possibly explaining the single uninjured mouse that responded strongly to denatonium + succinate in Fig. 4*A*. Nonetheless, the significant permeability increase observed only in post-infection mice underscores the involvement of SCCs in proinflammatory pathways. Whether this represents an adaptive or a pathological consequence of lung repair remains unclear.

Notably, activation of the tuft cell signaling circuit by parasite infection in the gut limits subsequent infection (27). It will be intriguing to see if SCC expansion in post-influenza lungs renders them resistant to subsequent infection with pathogens that are cleared by Th2 responses. Childhood respiratory virus infection predisposes individuals toward asthma, a Th2-associated disease, further suggesting possible involvement of SCCs (6, 11).

To the best of our knowledge, this study represents the first demonstration of a solitary chemosensory cell population that arises in the distal airways and alveoli after influenza virus infection. Our studies indicate a likely role for SCCs in mediating cross talk between inflammation and dysplasia, but there is a clear need for future studies to define more discrete functions of SCCs and the molecular mechanisms by which these functions are achieved.

ACKNOWLEDGMENTS

We thank Sriram Srivatsa and Katherine Geating for technical assistance.

GRANTS

This work was supported by National Institutes of Health Grants R00-HL-131817 to A. E. Vaughan and R01-DC-013588 to N. A. Cohen.

Fig. 3. Solitary chemosensory cells (SCCs) arise in post-influenza lungs. *A*: SCC-like cells expressing doublecortin-like kinase 1 (DCLK1) appear at ~12 days after influenza virus infection, with increasing numbers seen up to *day 51*. *B*: quantification of total number of SCCs relative to percentage of cytokeratin 5 (Krt5)-positive ($Krt5^+$) area. Values are means ± SE; $n = 3$ mice per group. *C*: schematic depicting lineage-mapping methodology; >99% of $DCLK1^+$ cells are completely traced ($tdTomato^{pos}$) in p63-CreERT2/tdTomato mice. *D*: quantification of lineage tracing by manual cell counts in tissue sections ($n = 3$ mice). *E*: RNA-sequencing analysis of post-influenza Krt5-traced cells (*day 17*) displayed increased expression of SCC-restricted genes, including several bitter taste receptors (Tas1r3, Tas2r108, Tas2r121, and Tas2r131). FPKM, fragments per kilobase of transcript per million mapped reads; Trpm5, transient receptor potential cation channel subfamily M member 5; Gnat3, G protein subunit-α transducin 3. *F*: influenza virus infection of Trpm5-GFP mice (*day 25*) resulted in green fluorescent protein (GFP)-positive cells in the lungs coexpressing DCLK1 (yellow/orange cells). Values are means ± SE; *n* is shown by individual dots on the plot, $n = 2$ per group. Scale bars, 50 μm.

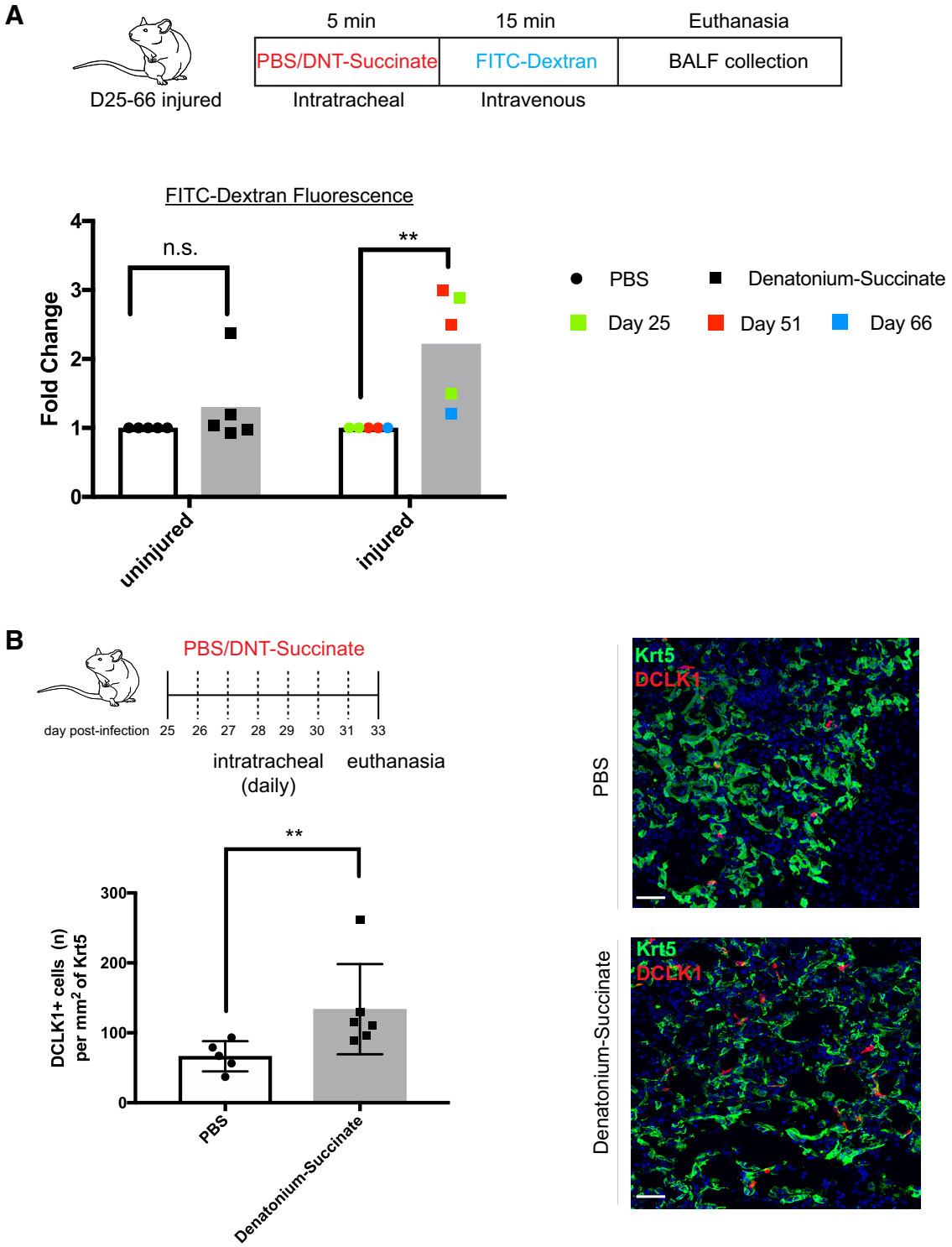

Fig. 4. Solitary chemosensory cell (SCC) activation promotes plasma extravasation into the air space and increased numbers of SCCs. *A*: schematic depicting plasma extravasation methodology; SCC activation by denatonium (DNT) + succinate triggers plasma extravasation, as observed by a significant increase in FITC-dextran fluorescence, shown as relative fluorescence intensity normalized to PBS-treated mice. Color-coded data points correspond to exact day of euthanasia post-infection. BALF, bronchoalveolar lavage fluid. Values are means ± SE; $n = 5$ mice per group. *B*: denatonium + succinate administration for 7 days triggers a significant increase in doublecortin-like kinase 1 (DCLK1)-positive SCCs in injured lungs (*day 33*). Krt5, cytokeratin 5. Values are means ± SE; $n = 5$ (PBS) and 6 (denatonium + succinate) mice. Scale bars, 50 μm. $^{**}P < 0.01$.

DISCLOSURES

No conflicts of interest, financial or otherwise, are declared by the authors.

AUTHOR CONTRIBUTIONS

C.K.R., D.R.H., N.A.C., and A.E.V. conceived and designed research; C.K.R., S.R.J., C.F.P., G.Z., A.I.W., N.N.P., and A.E.V. performed experiments; C.K.R. and A.E.V. analyzed data; C.K.R. and A.E.V. interpreted results of experiments; C.K.R. and A.E.V. prepared figures; C.K.R., D.R.H., N.A.C., and A.E.V. drafted manuscript; C.K.R., D.R.H., N.A.C., and A.E.V. edited and revised manuscript; C.K.R., D.R.H., N.A.C., and A.E.V. approved final version of manuscript.

REFERENCES

1. **Bankova LG, Dwyer DF, Yoshimoto E, Ualiyeva S, McGinty JW, Raff H, von Moltke J, Kanaoka Y, Frank Austen K, Barrett NA.** The cysteinyl leukotriene 3 receptor regulates expansion of IL-25-producing airway brush cells leading to type 2 inflammation. *Sci Immunol* 3: 3, 2018. doi:10.1126/sciimmunol.aat9453.
2. **Chen J, Wu J, Hao S, Yang M, Lu X, Chen X, Li L.** Long term outcomes in survivors of epidemic influenza A (H7N9) virus infection. *Sci Rep* 7: 17275, 2017. doi:10.1038/s41598-017-17497-6.
3. **Clapp TR, Medler KF, Damak S, Margolskee RF, Kinnamon SC.** Mouse taste cells with G protein-coupled taste receptors lack voltage-gated calcium channels and SNAP-25. *BMC Biol* 4: 7, 2006. doi:10.1186/1741-7007-4-7.
4. **Gerbe F, Sidot E, Smyth DJ, Ohmoto M, Matsumoto I, Dardalhon V, Cesses P, Garnier L, Pouzolles M, Brulin B, Bruschi M, Harcus Y, Zimmermann VS, Taylor N, Maizels RM, Jay P.** Intestinal epithelial tuft cells initiate type 2 mucosal immunity to helminth parasites. *Nature* 529: 226–230, 2016. doi:10.1038/nature16527.
5. **Howitt MR, Lavoie S, Michaud M, Blum AM, Tran SV, Weinstock JV, Gallini CA, Redding K, Margolskee RF, Osborne LC, Artis D, Garrett WS.** Tuft cells, taste-chemosensory cells, orchestrate parasite type 2 immunity in the gut. *Science* 351: 1329–1333, 2016. doi:10.1126/science.aaf1648.
6. **Jackson DJ, Gangnon RE, Evans MD, Roberg KA, Anderson EL, Pappas TE, Printz MC, Lee WM, Shult PA, Reisdorf E, Carlson-Dakes KT, Salazar LP, DaSilva DF, Tisler CJ, Gern JE, Lemanske RF Jr.** Wheezing rhinovirus illnesses in early life predict asthma development in high-risk children. *Am J Respir Crit Care Med* 178: 667–672, 2008. doi:10.1164/rccm.200802-309OC.
7. **Keeler SP, Agapov EV, Hinojosa ME, Letvin AN, Wu K, Holtzman MJ.** Influenza A virus infection causes chronic lung disease linked to sites of active viral RNA remnants. *J Immunol* 201: 2354–2368, 2018. doi:10.4049/jimmunol.1800671.
8. **Kohanski MA, Workman AD, Patel NN, Hung L-Y, Shtraks JP, Chen B, Blasetti M, Doghramji L, Kennedy DW, Adappa ND, Palmer JN, Herbert DR, Cohen NA.** Solitary chemosensory cells are a primary epithelial source of IL-25 in patients with chronic rhinosinusitis with nasal polyps. *J Allergy Clin Immunol* 142: 460–469.e7, 2018. doi:10.1016/j.jaci.2018.03.019.
9. **Koppe S, Túlio AIB, Villegas ILP, Motter AA.** Pulmonary function in patients with pandemic H1N1. *Fisioter Mov* 29: 805–812, 2016. doi:10.1590/1980-5918.029.004.ao17.
10. **Kumar PA, Hu Y, Yamamoto Y, Hoe NB, Wei TS, Mu D, Sun Y, Joo LS, Dagher R, Zielonka EM, Wang Y, Lim B, Chow VT, Crum CP, Xian W, McKeon F.** Distal airway stem cells yield alveoli in vitro and during lung regeneration following H1N1 influenza infection. *Cell* 147: 525–538, 2011. doi:10.1016/j.cell.2011.10.001.
11. **Kusel MM, de Klerk NH, Kebadze T, Vohma V, Holt PG, Johnston SL, Sly PD.** Early-life respiratory viral infections, atopic sensitization, and risk of subsequent development of persistent asthma. *J Allergy Clin Immunol* 119: 1105–1110, 2007. doi:10.1016/j.jaci.2006.12.669.
12. **Lee D-K, Liu Y, Liao L, Wang F, Xu J.** The prostate basal cell (BC) heterogeneity and the p63-positive BC differentiation spectrum in mice. *Int J Biol Sci* 10: 1007–1017, 2014. doi:10.7150/ijbs.9997.
13. **Lee RJ, Hariri BM, McMahon DB, Chen B, Doghramji L, Adappa ND, Palmer JN, Kennedy DW, Jiang P, Margolskee RF, Cohen NA.** Bacterial D-amino acids suppress sinonasal innate immunity through sweet taste receptors in solitary chemosensory cells. *Sci Signaling* pii: eaam7703, 2017. doi:10.1126/scisignal.aam7703.
14. **Lee RJ, Kofonow JM, Rosen PL, Siebert AP, Chen B, Doghramji L, Xiong G, Adappa ND, Palmer JN, Kennedy DW, Kreindler JL, Margolskee RF, Cohen NA.** Bitter and sweet taste receptors regulate human upper respiratory innate immunity. *J Clin Invest* 124: 1393–1405, 2014. doi:10.1172/JCI72094.
15. **Lei W, Ren W, Ohmoto M, Urban JF Jr, Matsumoto I, Margolskee RF, Jiang P.** Activation of intestinal tuft cell-expressed Sucnr1 triggers type 2 immunity in the mouse small intestine. *Proc Natl Acad Sci USA* 115: 5552–5557, 2018. doi:10.1073/pnas.1720758115.
16. **Lin W, Ogura T, Margolskee RF, Finger TE, Restrepo D.** TRPM5-expressing solitary chemosensory cells respond to odorous irritants. *J Neurophysiol* 99: 1451–1460, 2008. doi:10.1152/jn.01195.2007.
17. **Liu W, Peng L, Liu H, Hua S.** Pulmonary function and clinical manifestations of patients infected with mild influenza A virus subtype H1N1: a one-year follow-up. *PLoS One* 10: e0133698, 2015. doi:10.1371/journal.pone.0133698.
18. **Madisen L, Zwingman TA, Sunkin SM, Oh SW, Zariwala HA, Gu H, Ng LL, Palmiter RD, Hawrylycz MJ, Jones AR, Lein ES, Zeng H.** A robust and high-throughput Cre reporting and characterization system for the whole mouse brain. *Nat Neurosci* 13: 133–140, 2010. doi:10.1038/nn.2467.
19. **Monticelli LA, Sonnenberg GF, Abt MC, Alenghat T, Ziegler CGK, Doering TA, Angelosanto JM, Laidlaw BJ, Yang CY, Sathaliyawala T, Kubota M, Turner D, Diamond JM, Goldrath AW, Farber DL, Collman RG, Wherry EJ, Artis D.** Innate lymphoid cells promote lung tissue homeostasis following acute influenza virus infection. *Nat Immunol* 12: 1045–1054, 2011. doi:10.1038/ni.2131.
20. **Montoro DT, Haber AL, Biton M, Vinarsky V, Lin B, Birket SE, Yuan F, Chen S, Leung HM, Villoria J, Rogel N, Burgin G, Tsankov AM, Waghray A, Slyper M, Waldman J, Nguyen L, Dionne D, Rozenblatt-Rosen O, Tata PR, Mou H, Shivaraju M, Bihler H, Mense M, Tearney GJ, Rowe SM, Engelhardt JF, Regev A, Rajagopal J.** A revised airway epithelial hierarchy includes CFTR-expressing ionocytes. *Nature* 560: 319–324, 2018. doi:10.1038/s41586-018-0393-7.
21. **Moyron-Quiroz JE, Rangel-Moreno J, Kusser K, Hartson L, Sprague F, Goodrich S, Woodland DL, Lund FE, Randall TD.** Role of inducible bronchus associated lymphoid tissue (iBALT) in respiratory immunity. *Nat Med* 10: 927–934, 2004. doi:10.1038/nm1091.
22. **Nadjsombati MS, McGinty JW, Lyons-Cohen MR, Jaffe JB, DiPeso L, Schneider C, Miller CN, Pollack JL, Nagana Gowda GA, Fontana MF, Erle DJ, Anderson MS, Locksley RM, Raftery D, von Moltke J.** Detection of succinate by intestinal tuft cells triggers a type 2 innate immune circuit. *Immunity* 49: 33–41.e7, 2018. doi:10.1016/j.immuni.2018.06.016.
23. **Patel NN, Kohanski MA, Maina IW, Triantafillou V, Workman AD, Tong CCL, Kuan EC, Bosso JV, Adappa ND, Palmer JN, Herbert DR, Cohen NA.** Solitary chemosensory cells producing interleukin-25 and group-2 innate lymphoid cells are enriched in chronic rhinosinusitis with nasal polyps. *Int Forum Allergy Rhinol* 8: 900–906, 2018. doi:10.1002/alr.22142.
24. **Saunders CJ, Christensen M, Finger TE, Tizzano M.** Cholinergic neurotransmission links solitary chemosensory cells to nasal inflammation. *Proc Natl Acad Sci USA* 111: 6075–6080, 2014. doi:10.1073/pnas.1402251111.
25. **Schneider C, O'Leary CE, von Moltke J, Liang HE, Ang QY, Turnbaugh PJ, Radhakrishnan S, Pellizzon M, Ma A, Locksley RM.** A metabolite-triggered tuft cell-ILC2 circuit drives small intestinal remodeling. *Cell* 174: 271–284.e14, 2018. doi:10.1016/j.cell.2018.05.014.
26. **Short KR, Kroeze EJBV, Fouchier RAM, Kuiken T.** Pathogenesis of influenza-induced acute respiratory distress syndrome. *Lancet Infect Dis* 14: 57–69, 2014. doi:10.1016/S1473-3099(13)70286-X.
27. **Tata PR, Chow RD, Saladi SV, Tata A, Konkimalla A, Bara A, Montoro D, Hariri LP, Shih AR, Mino-Kenudson M, Mou H, Kimura S, Ellisen LW, Rajagopal J.** Developmental history provides a roadmap for the emergence of tumor plasticity. *Dev Cell* 44: 679–693.e5, 2018. doi:10.1016/j.devcel.2018.02.024.
28. **Taylor MS, Chivukula RR, Myers LC, Jeck WR, Waghray A, Tata PR, Selig MK, O'Donnell WJ, Farver CF, Thompson BT, Rajagopal J, Kradin RL.** A conserved distal lung regenerative pathway in acute lung injury. *Am J Pathol* 188: 1149–1160, 2018. doi:10.1016/j.ajpath.2018.01.021.
29. **Tizzano M, Gulbransen BD, Vandenbeuch A, Clapp TR, Herman JP, Sibhatu HM, Churchill ME, Silver WL, Kinnamon SC, Finger TE.** Nasal chemosensory cells use bitter taste signaling to detect irritants and bacterial signals. *Proc Natl Acad Sci USA* 107: 3210–3215, 2010. doi:10.1073/pnas.0911934107.

32. **Vaughan AE, Brumwell AN, Xi Y, Gotts JE, Brownfield DG, Treutlein B, Tan K, Tan V, Liu FC, Looney MR, Matthay MA, Rock JR, Chapman HA.** Lineage-negative progenitors mobilize to regenerate lung epithelium after major injury. *Nature* 517: 621–625, 2015. doi:10.1038/nature14112.
33. **von Moltke J, Ji M, Liang HE, Locksley RM.** Tuft-cell-derived IL-25 regulates an intestinal ILC2-epithelial response circuit. *Nature* 529: 221–225, 2016. doi:10.1038/nature16161.
33a. **World Health Organization.** *WHO Guidelines on the Use of Vaccines and Antivirals During Influenza Pandemics*. https://www.who.int/csr/resources/publications/influenza/WHO_CDS_CSR_RMD_2004_8/en/.
34. **Xi Y, Kim T, Brumwell AN, Driver IH, Wei Y, Tan V, Jackson JR, Xu J, Lee DK, Gotts JE, Matthay MA, Shannon JM, Chapman HA, Vaughan AE.** Local lung hypoxia determines epithelial fate decisions during alveolar regeneration. *Nat Cell Biol* 19: 904–914, 2017. doi:10.1038/ncb3580.
35. **Yang Y, Riccio P, Schotsaert M, Mori M, Lu J, Lee D-K, García-Sastre A, Xu J, Cardoso WV.** Spatial-temporal lineage restrictions of embryonic p63^{+} progenitors establish distinct stem cell pools in adult airways. *Dev Cell* 44: 752–761.e4, 2018. doi:10.1016/j.devcel.2018.03.001.
36. **Zacharias WJ, Frank DB, Zepp JA, Morley MP, Alkhaleel FA, Kong J, Zhou S, Cantu E, Morrisey EE.** Regeneration of the lung alveolus by an evolutionarily conserved epithelial progenitor. *Nature* 555: 251–255, 2018. doi:10.1038/nature25786.